VALIDATION OF CFD-BWR, A NEW TWO-PHASE COMPUTATIONAL FLUID DYNAMICS MODEL FOR BOILING WATER REACTOR ANALYSIS

V.Ustinenko[1], M.Samigulin[1], A.Ioilev[1], S.Lo[2], A.Tentner[3], A.Lychagin[4], A.Razin[4], V.Girin[4], Ye.Vanyukov[4]

1 - Institute of Theoretical and Mathematical Physics, Russian Federal Nuclear Center (VNIIEF), Russian Federation
2 - CD-adapco, UK
3 - Argonne National Laboratory, USA
4 – Sarov Laboratories, Russian Federation

Abstract

To allow the detailed analysis of the two-phase coolant flow and heat transfer phenomena in a Boiling Water Reactor fuel bundle the CFD-BWR model is being developed for use with the commercial code STAR-CD which provides general two-phase flow modeling capabilities. The paper reviews the key boiling phenomenological models, describes the overall strategy adopted for the combined CFD-BWR and STAR-CD boiling models validation and presents results of a set of experiment analyses focused on the validation of specific models implemented in the code. The location of vapor generation onset, axial temperature profile and axial and radial void distributions were calculated and compared with experimental data. Good agreement between computed and measured results was obtained for a large number of test cases.

KEYWORDS: Boiling Water Reactor, Two-Phase Flow, Conjugate Heat Transfer, Computational Fluid Dynamics.

Introduction

This paper presents the validation strategy and validation results obtained during the development of an advanced Computational Fluid Dynamics (CFD) computer code (CFD-BWR) that allows the detailed analysis of the two-phase flow and heat transfer phenomena in a Boiling Water Reactor (BWR) fuel bundle. The CFD-BWR code is being developed as a customized module built on the foundation of the commercial CFD-code STAR-CD which provides general two-phase flow modeling capabilities. We have described in [1] the model development strategy that has been adopted by the development team for the prediction of boiling flow phenomena in a BWR fuel bundle. The strategy includes the use of local inter-phase surface topology map and topology specific phenomenological models in conjunction with an interface transport and topology transport approach. This paper reviews the key boiling phenomenological models implemented to date, describes the overall validation strategy adopted for the STAR-CD with CFD-BWR module and presents results of experiment analyses focused on the validation of specific models implemented in the code.

1. Overview of Two-Phase Models

The two-phase flow models implemented in the CFD-BWR code can be grouped into three broad categories: models describing the vapor generation at the heated cladding surface, models describing the interactions between the vapor and the liquid coolant, and models describing the heat transfer between the fuel pin and the two-phase coolant. These models have been described in Refs. [1, 2] and will be briefly reviewed in this section of the paper. The boiling model was recently expanded to include conjugate heat transfer so that the complete heat transfer system, including the heat conduction in the fuel and cladding, can be studied. The ability of computing the solid fuel and cladding temperatures is important in analyses of critical heat flux (CHF), and is also required for the coupling of the thermal-hydraulic models with neutronic models.

1.1 Transport Equations

The STAR-CD Eulerian two-phase solver tracks the mass, momentum, and energy of the liquid and vapor phases in each computational cell. Full details of the Eulerian two-phase flow models in STAR-CD can be found in Refs. [3, 4]. The main equations solved are the conservation of mass, momentum and energy for each phase.

The conservation of mass equation for phase k is:

$$\frac{\partial}{\partial t}\left(\alpha_k \rho_k\right) + \nabla.\left(\alpha_k \rho_k u_k\right) = \dot{m}_{ki} - \dot{m}_{ik} . \tag{1}$$

The conservation of momentum equation for phase k is:

$$\frac{\partial}{\partial t}\left(\alpha_k \rho_k u_k\right) + \nabla.\left(\alpha_k \rho_k u_k u_k\right) - \nabla.\left(\alpha_k\left(\tau_k + \tau_k^t\right)\right) = -\alpha_k \nabla p + \alpha_k \rho_k g + M . \tag{2}$$

The conservation of energy equation for phase k is:

$$\frac{\partial}{\partial t}\left(\alpha_k \rho_k e_k\right) + \nabla.\left(\alpha_k \rho_k u_k e_k\right) - \nabla.\left(\alpha_k \lambda_k \nabla T_k\right) = Q . \tag{3}$$

The inter-phase forces considered in the model are: drag, turbulent dispersion, virtual mass and lift forces, and momentum transfer associated with mass transfer, hence

$$M = F_D + F_T + F_M + F_L + \dot{m}_{ki} u_i - \dot{m}_{ik} u_k \tag{4}$$

An extended k-ε model containing extra source terms that arise from the inter-phase forces present in the momentum equations is used to model turbulence in the flow. Further details of the inter-phase forces can be found in Refs. [2, 3, 4].

The lift force and the wall lubrication force are found to be important in obtaining correct radial distribution of the two phases. The correlation suggested in Ref. [5] is used for the lift force, in which lift force depends on bubble size D_b as derived in Ref. [6]. According to this correlation, the lift force depends on Eötvos number *Eö*:

$$F_L = C_{lift}\alpha_d \rho_c (u_d - u_c) \times \nabla \times u_c \tag{5}$$

$$C_{lift} = C_{LF} + C_{WK}, \tag{6}$$

Where:

$$C_{LF} = 0.288 \cdot tanh(0.121 \cdot \mathrm{Re}_d), \tag{7}$$

$$C_{WK} = \begin{cases} 0, & \text{Eö} < 4 \\ -0.096\text{Eö} + 0.384, & 4 < \text{Eö} < 10 \\ -0.576 & \text{Eö} > 10 \end{cases}. \tag{8}$$

$\mathrm{Re}_d = \dfrac{|u_d - u_c| \cdot D_b}{\nu_c}$ is the Reynolds number, $\text{Eö} = \dfrac{g \cdot (\rho_c - \rho_d) \cdot D_b^2}{\sigma_{ten}}$ is the Eötvos number, g_0 is the gravitational acceleration and σ_{ten} is surface tension coefficient, indexes c and d denotes continuous and disperse phases.

The wall lubrication force is modeled as in refs. [7, 8]:

$$F_{wg} = -F_{wl} = -\xi_b \cdot \zeta_b \cdot \frac{\alpha_g \cdot \rho_l \cdot |u_g - u_l|^2}{D_b} \cdot \max\left\{C_{w1} + C_{w2}\frac{D_b}{y}, 0\right\} \cdot n_w \tag{9}$$

where y is the distance to the nearest wall, n_w is the unit normal pointing away from the wall, and C_{w1} and C_{w2} are coefficients.

A validation exercise specifically addressing the effects of the lift and wall lubrication force on the radial distribution of bubbles is described below in Section 2.

1.2 Boiling model

The inter-phase heat and mass transfer models were obtained by considering the heat transfers from the gas and the liquid to the gas/liquid interface, see Fig. 1. The net heat transfer to the interface is used to compute the mass transfer rate between the two phases.

Heat transfer rate from the liquid to the interface is:

$$\dot{q}_l = h_l A_d (T_l - T_{sat}). \tag{10}$$

Heat transfer rate from the gas to the interface is:

$$\dot{q}_g = h_g A_d (T_g - T_{sat}). \tag{11}$$

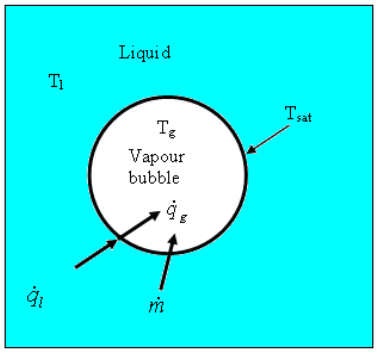

Fig.1. Heat and mass transfer between a vapor bubble and liquid

The heat transferred to the interface is calculated using Eqs. 10 and 11 and used to determine the inter-phase mass transfer (i.e. evaporation or condensation) rate:

$$\dot{m} = \frac{\dot{q}_l + \dot{q}_g}{h_{fg}}. \tag{12}$$

1.3 Wall Heat Transfer Model

A model describing the heat transfer between the heated wall and the coolant has also been developed. The heat flux from the wall is divided into three parts according to a wall heat partitioning model which includes convective heat for the liquid, evaporative heat for generation of steam and quench heat for heating of liquid in the nucleation sites. The details of the boiling model and the wall heat partitioning model can be found in Refs. [1-4]. In coupling the flow analysis with neutronics, temperatures of the fuel the cladding of the fuel pins must be determined together with the fluid temperatures as a conjugate heat transfer (CHT) problem. Heat transfer within the solids can be described by the following energy equation:

$$\frac{\partial(\rho e)}{\partial t} = \frac{\partial}{\partial x_j}\left(\lambda_{ji}\frac{\partial T}{\partial x_j}\right) + s_e, \tag{13}$$

where s_e is the fission heat source obtained from the neutronic code.

Equation (13) is solved together with the energy equation for the fluid (3). From the calculation the temperature at the solid/fluid interface is obtained. When this wall temperature is greater than the saturation temperature, the boiling model described above is applied on the fluid side to produce vapor.

2. Two-Phase Model Validation Strategy

Empirical correlations are used in the models described above hence validation checks of the computed solutions against experimental data are essential and must be carried out. A comprehensive validation strategy has been developed which includes both validation analyses focused on individual phenomenological models and integral test analyses including a combination of two-phase phenomena characteristic for BWR fuel assemblies. No new experiments are planned as part of this work, but a wealth of experimental data focused on various phenomenological aspects of two-phase flows has been published in scientific journals and will be used for the validation of the CFD-BWR code. An extensive literature review has been conducted and 24 papers describing experiments that can be used as test cases for the validation of the STAR-CD code and the CFD-BWR module have been selected. These test-cases provide a validation basis for a variety of two-phase flow phenomena already modeled and have been grouped in the following way:

A - Adiabatic flow of two-phase steam-water and air-water mixture experiments, for the validation of interfacial drag and wall friction models;

B - Surface **Boiling** experiments, for the validation of models for boiling, inter-phase heat and mass transfer, surface heat transfer, surface drag during boiling, boiling crisis;

C – Steam **Condensation** experiments for the validation of inter-phase heat and mass transfer models and interfacial drag models;

D - Dispersed flow of water droplets in steam experiments, for the validation of models for inter-phase heat and mass transfer, droplet deposition on heated surfaces, and surface heat transfer;

I - Integral experiments in which several two-phase flow regimes occur, so this data can be used to validate the flow regime map and the interaction between multiple phenomenological models;

M – **Model** experiments in which two-phase flow in bundles of uniformly and non-uniformly heated fuel rods are studied, which can be used for the benchmarking of models and the code under conditions representative of BWR operating conditions.

Multiple experiments from the list presented above have been already analyzed as part of the model validation effort, and the results of several experiment analyses are presented. The location of vapor generation onset, axial temperature profile and axial and radial void distributions were calculated and compared with experimental data. As the code calculates detailed three-dimensional distributions of void fraction, temperature, and velocity fields, comparison with experimental data sometimes requires the aggregation of calculated local results. For example, the void fraction at a given axial location may be measured as a channel average depending on the measurement technique, and a corresponding average must be constructed from the calculated local values for direct comparison. Good agreement between computed and measured results was obtained for a large number of test-cases.

2.1 Validation Series A

Numerical simulation results obtained for air-water bubbly flow in vertical pipes under atmospheric pressure at room temperature can be given as an example; relevant experimental data are given in Refs. [7, 9-11]. Radial distributions of liquid and air velocity and void fraction were measured in these experiments.

A schematic of the Wang, et al., experiments [7] is shown in Fig. 2. The water-air bubbly mixture was obtained in the mixing tee. In the experiments, volumetric fluxes of the phases and mean bubble diameter were measured at the inlet, and radial distributions of liquid velocity and void fraction were measured in a cross section near outlet. The experiments were performed with a pipe of diameter 57.15 mm. A schematic of the Liu experiments [8] and Serizawa experiments [9] is the same as shown in Fig. 2, except for different pipe diameter 57.2 mm and 60 mm, respectively.

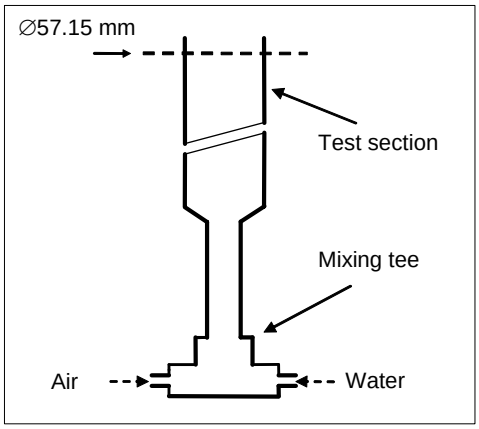

Fig.2. Schematic of experiment for study of air-water bubbly flow

Input data for the test-case calculations taken mainly from Ref. [7]. The length of the experimental pipe is not given in papers [9, 10], so the pipe length was set to 10 m in our calculations, as in calculations of Troshko and Hassan [7]. The length of the pipe is 2.15 m in Serizawa experiments [11]. The calculations conducted show that flow settles rather quickly: at ~2 m from inlet of the test section. All three sets of experiments were conducted at atmospheric pressure and room temperature.

Figures below show a comparison between experimental data and numerical results computed in a standard set-up STAR-CD simulation (C_{lift}=0.25), with close to zero coefficient C_{lift}=-0.025, and with the lift force represented as a function of Eötvos number. The following coefficients from Ref. [8] were used for the wall lubrication force: C_{W1}=-0.06 and C_{W2}=0.147. In Figs. 3-5 W1 denotes the Wang, et al., experiment #1 [9], L8 denotes the Liu experiment #8 [10], and S2 denotes the Serizawa, et al., experiment #2 [11]; parameters of mixture at inlet (superficial velocity of liquid J_l and gas J_g, and volume fraction of gas α) are presented in Table 1. As in calculations of Troshko and

Hassan [7], the bubble diameter used in our calculations was taken D_b=2.8 mm for simulations of both the Liu experiment and the Wang, et al., experiment. In simulation of Serizawa experiment bubble diameter D_b=4 mm was used.

Using of lift force as a function of Eötvos number provides good correspondence of simulated void fraction radial distribution to experimental data, including the near wall peak. Note also improvement in the axial liquid and air velocity radial distributions in calculations using this model.

Table 1 - Parameters of mixture at inlet

Experiment	J_l, m/s	J_g, m/s	α
W1	0.43	0.1	0.132
L8	1.0	0.1	0.106
S2	1.03	0.151	0.102

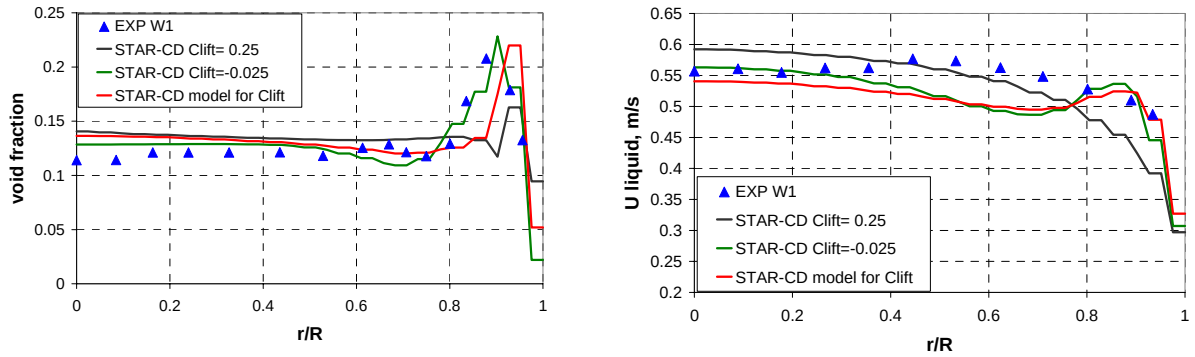

Fig.3. Numerical and experimental void fraction and water velocity as a function of dimensionless radial distance for experiment W1 [7, 9]

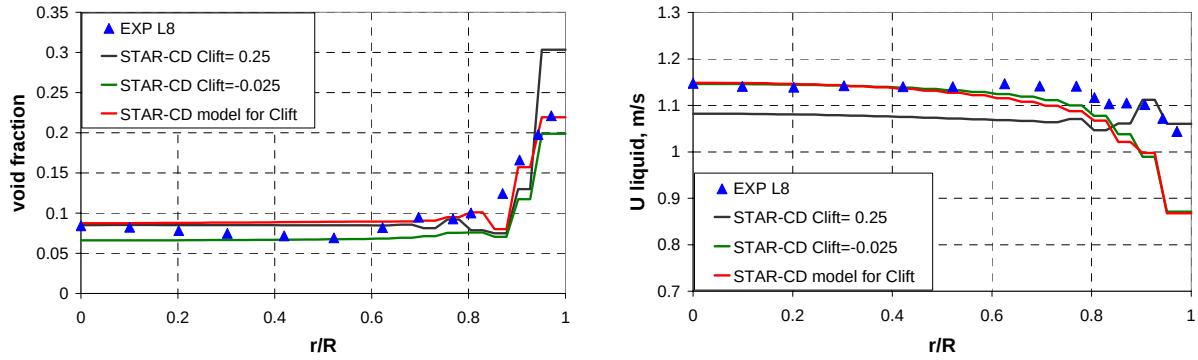

Fig.4. Numerical and experimental void fraction and water velocity as a function of dimensionless radial distance for experiment L8 [7, 10]

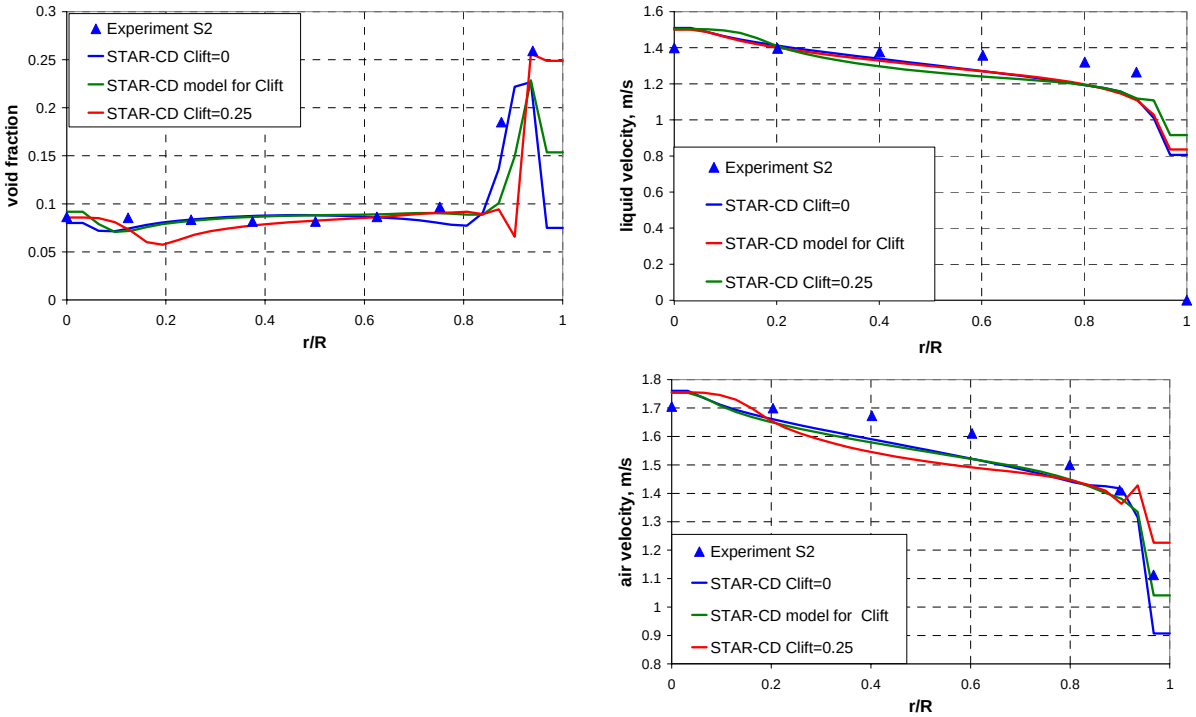

Fig.5. Numerical and experimental void fraction and water and air velocity as a function of dimensionless radial distance for experiment S2 [7, 11]

2.2 ***Validation Series B***

Bartolomei, et al., experiments

The bubbly-flow boiling model was also used for the analysis of Bartolomei et al. experiments [12, 13]. The set-up of experiments is illustrated schematically in Fig. 6. In these experiments the average cross-section void fraction was measured over the pipe length in upward water flow. In the heated lower section of the pipe sub-cooled boiling occurs and steam is generated. The section above is adiabatic and vapor condensation occurs due to the mixing of the vapor generated near the heated wall in the lower section with the still subcooled liquid core. The pipe diameter is 12.03 mm, the heated section length is L_0=1 m and the total pipe length is L=1.4 m.

In these calculations we used the same models as in described above ones except for the bubble size, for which we used Kurul-Podowski correlation [14] with bubble size dependent on liquid subcooling.

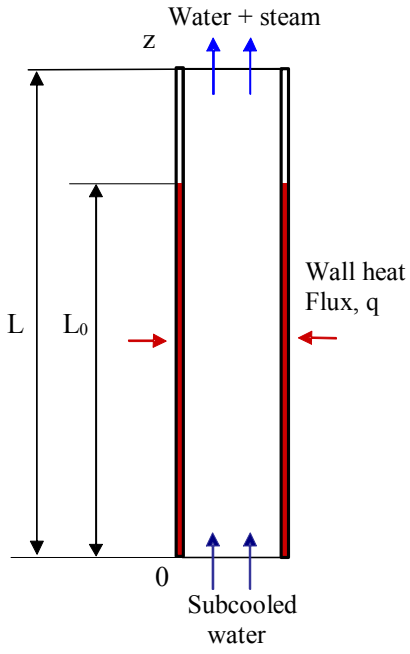

Fig. 6. Schematic of experimental section for study of boiling and condensation

Subcooled water at temperature T_l enters the pipe at pressure P_l=6.89 MPa and mass flux G_l. Heat flux at the channel wall in the heated section of the pipe is q=const. Saturation temperature for these conditions is T_{sat}=558 K. Values of T_l, G_l, q and subcooling ΔT_{sub} for the experiments discussed are presented in Table 2. The wall heat boundary condition in the non-heated upper section of the pipe is q=0.

Table 2. Parameters of experimental set-up

Experiment #	q, MW/m^2	G_l, kg/(m^2·s)	T_l, K	ΔT_{sub}, K
2	1.2	1500	495	63
3	0.8	1500	519	39
5	0.8	1000	503	55

Typical distributions of the water temperature and void fraction calculated for experiment # 2 are presented in Figs. 7a and 7b, respectively. Figs. 8a and 8b show the void fraction and water temperature radial distribution, respectively, calculated for experiment # 2 at three axial locations. The elevation of 0.6 m corresponds to the beginning of boiling, elevation of 0.95 m is located near the end of the heated section in the boiling region, and elevation of 1.3 m is located near the end of the experimental section in the condensation region.

Figs. 7 and 8 illustrate development of radial heating of water, changing of void fraction and transport of steam due to lift and turbulent dispersion forces. By the end of the heated section the water near the heated wall reaches saturation temperature, while the water at the center of the pipe remains approximately 30K sub-cooled. As illustrated in Fig. 8a, the vapor fraction decreases in the adiabatic section of the pipe due to condensation caused by turbulent mixing of the two-phase mixture from the near-wall region with the sub-cooled liquid in the central region. Correspondingly, the radial distribution of water temperature in the condensation section flattens mainly due to turbulent transport, as illustrated in Fig. 8b. Comparison between the calculated bulk void fraction distribution and the corresponding experimental data is presented in Fig. 9. The experimental and numerical profiles of void fraction are in reasonably good agreement, although the discrepancy in some sections is up to ~30%.

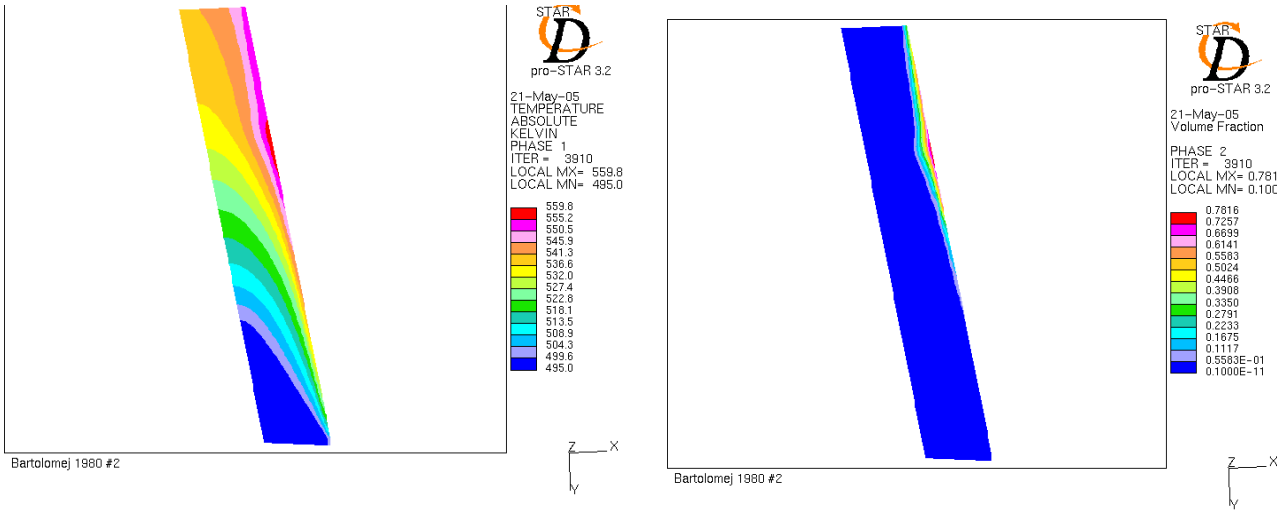

Fig.7. a. Distribution of water temperature and b. Void fraction in the flow (simulation of experiment #2)

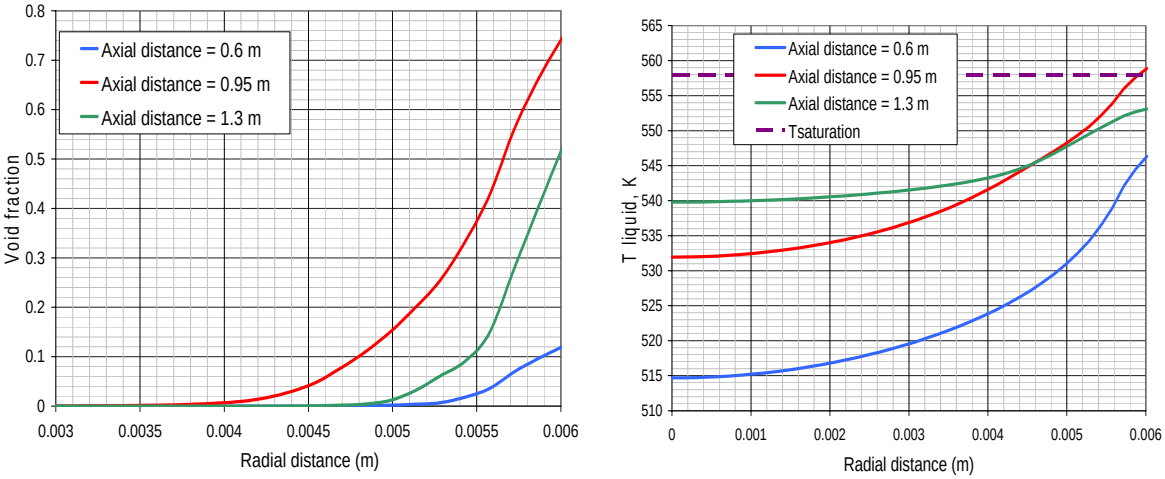

Fig.8 Radial distribution of: a. void fraction and b. water temperature at three axial locations (simulation of experiment # 2)

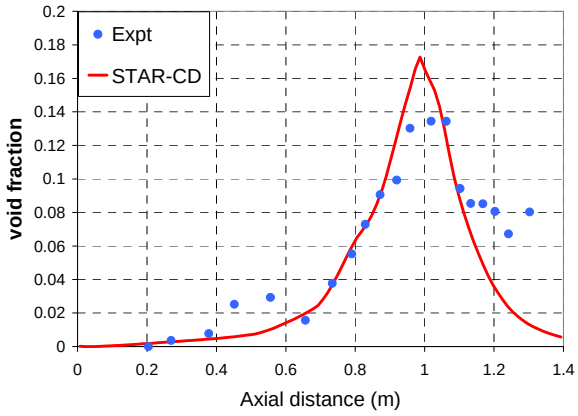

Experiment #2

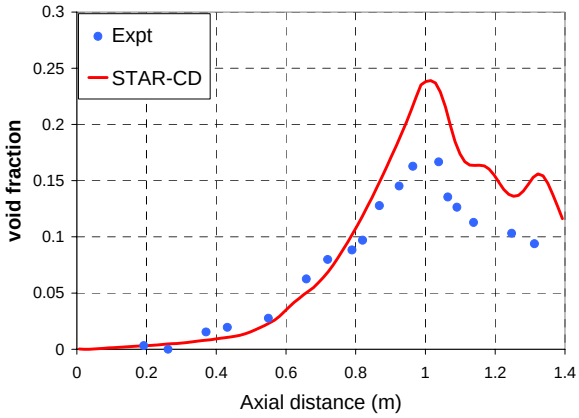

Experiment #3

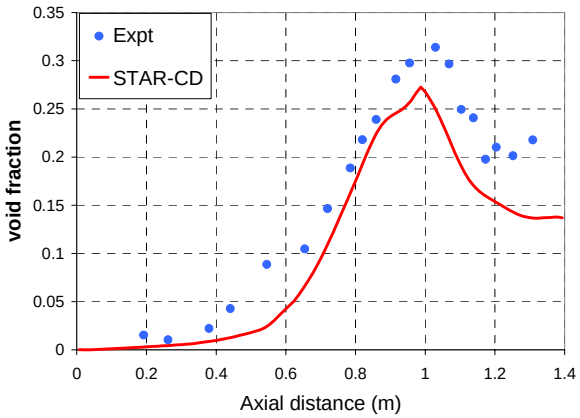

Experiment #5

Fig.9. Average void fraction as a function of distance along the pipe

Good qualitative agreement was obtained for simulation of experiment #2. Simulations of experiments #3 and #5 tend to over-predict and under-predict the void fraction, respectively. This suggests that vaporization and condensation models should be improved to handle a wider range of flow parameters in the same manner. Overall rather good agreement between numerical and experimental data was obtained in calculations for boiling and condensation processes.

Lee, Park and Lee and Tu and Yeoh experiments

Radial distribution of void fraction in a vertical (concentric) annulus in flow of subcooled boiling water was studied in experiments of Lee, Park and Lee [15] and Tu and Yeoh [16-17]. Schematic of the experimental section is presented in Fig. 10. The experimental section is made as an annulus with inner diameter 19 mm, 37.5 mm, length 2.376 m and heated section of the inner pipe 1.67 m in length. Subcooled water is fed upwards. Measurements of radial distribution of local void fraction and steam velocity were taken using two-conductivity probe method, and water velocity distributions were measured by the Pitot tube method. The measurements were taken in a single measurement section located at the elevation of 1.61 m from the inlet. The experiments were carried out with variable mass flux G_l=476-1061 kg/(m^{2}s), heat flux q=114.8-320.4 kW/m^2, outlet pressure P=1-2 bar and inlet subcooling ΔT_{sub}=11.5-21.3 K. Simulation was performed for the experiments with q=152.3 kW/m^2, G_l=474 kg/(m^{2}s), P=0.14 MPa (saturation temperature T_{sat}=383 K), ΔT_{sub}=13.4 K.

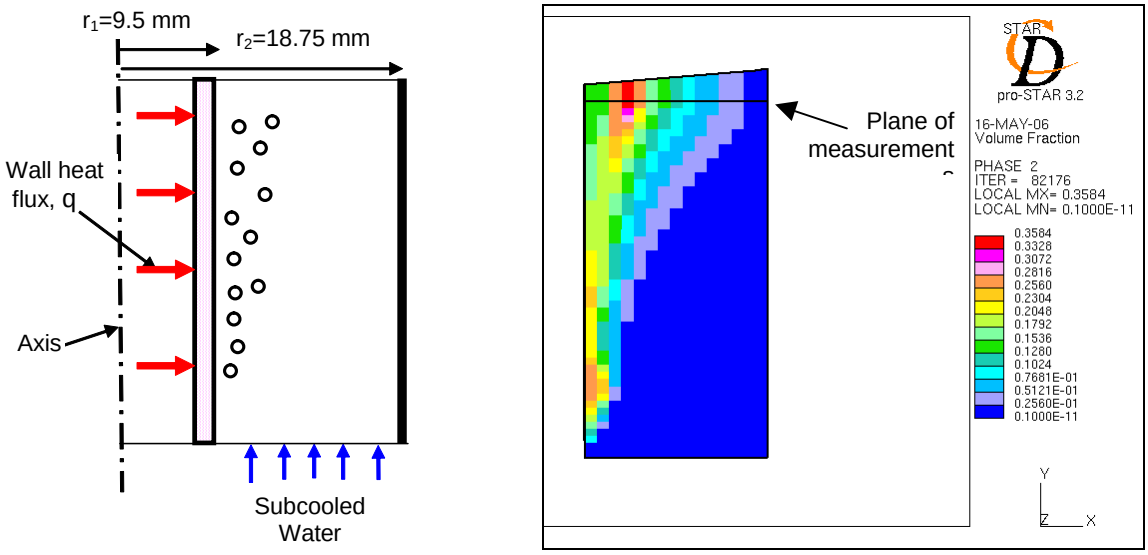

Fig.10. Schematic of the experimental section for study of boiling in annular channel and calculated vapor distribution

Calculations were performed using standard STAR-CD models with turbulence, turbulent dispersion force, virtual mass with the coefficient C_{VM}=0.5, interfacial drag (Wang curve fit [3]), buoyancy, no slip for water and slip for vapor. Simulations were performed using three different models of the lift force: a) a standard setup STAR-CD simulation with C_{lift}=0.25, b) negative coefficient C_{lift}=-0.025, -0.25 and -0.5, and c) with the lift force represented as a function of Eötvos number given by Eqns. (5-8). The following coefficients from Ref. [8] were used for wall lubrication force: C_{W1}=-0.06 and C_{W2}=0.147. Correlation of Kurul and Podowski [14] with parameters d_0=10^{-4}, d_1=4·10^{-3} m was used for the bubble diameter dependence on liquid subcooling.

Simulated distribution of void fraction (calculation with C_{lift}=-0.5) is presented in Fig. 10. Radial distributions of void fraction (calculations with C_{lift}=-0.025, -0.25 and -0.5) and phases axial velocities

(calculation with C_{lift}=-0.5) are presented in Fig. 11. Close agreement of results of calculations with experimental data was obtained by using C_{lift}=-0.25 and -0.5. With the lift force represented as a function of Eötvos number the results are close to the calculation with C_{lift}=-0.025. The reason may be in larger bubble size that took place in the experiment (~5 mm). As could be seen from Eqns. (5-8), the lift force depends on Eötvos number *Eö* and changes its direction when bubble size exceeds a critical value.

Comparing this to simulations described above in *Validation Series A* it can be seen that different values of C_{lift} are needed for surface boiling and adiabatic flow to get agreement with experimental data. So, development of the lift force model should be continued.

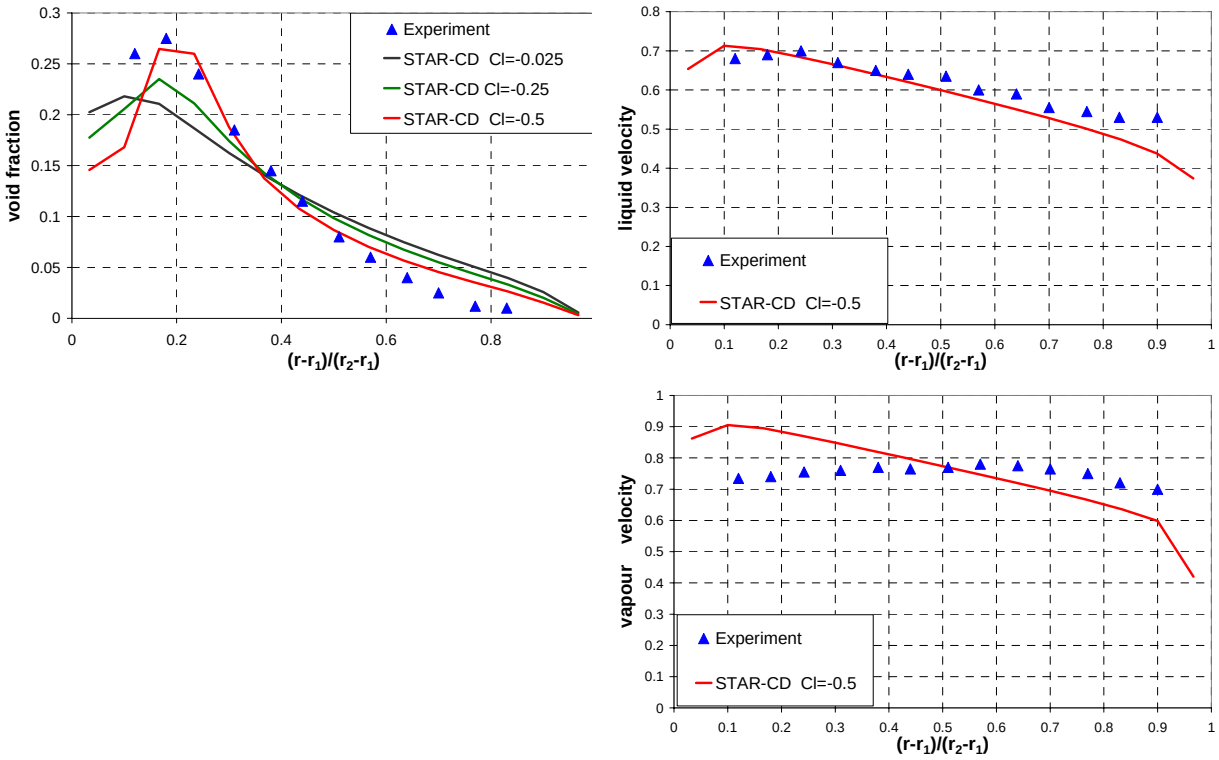

Fig.11. Numerical and experimental void fraction and water and vapor velocity as a function of dimensionless radial distance

Khlopushin, Tarasova and Boronina experiments

Wall friction in surface-boiling water flow in a vertical channel was studied in Khlopushin, Tarasova and Boronina experiments [18]. In these experiments illustrated schematically in Fig. 12, subcooled water is fed upwards into vertical pipe of inner radius 4.125 mm and length 0.5 m. The pipe wall is heated by direct electric current. Each series of tests was carried out at constant pressure, mass flux and heating. Inlet water subcooling was varied. Regimes without surface boiling developed first, then followed regimes with gradually increasing surface boiling length. A test series was finished when outlet water nearly reached saturation temperature under the conditions of the experiment. Inlet water temperature, heating and mass flux were varied for different experiments, and the length of section with surface boiling and pressure drop along this section were measured in the experiments.
Aim of numerical simulations is to compare numerical results on drag as a function of water sub-cooling to experimental data (pressure drop in the pipe as a function of the section with surface boiling). Calculations were performed for pressure is P=2.45 MPa, wall heat flux q=0.625 MW/m^2,

inlet mass flux of water G_l =2000 kg/(m^2·s), saturation temperature T_{sat}=496 K. The other parameters of this problem are given below. All calculations were performed using standard STAR-CD models with turbulence, turbulent dispersion force, virtual mass with the coefficient C_{VM}=0.5, lift force with the coefficient C_{lift}=0.25, and interfacial drag (Wang curve fit [3]). Bubble diameter was set to D_b=1 mm. A comparison between numerical and experimental data is given in Fig. 13. Overall rather good agreement between numerical and experimental data was obtained in calculations.

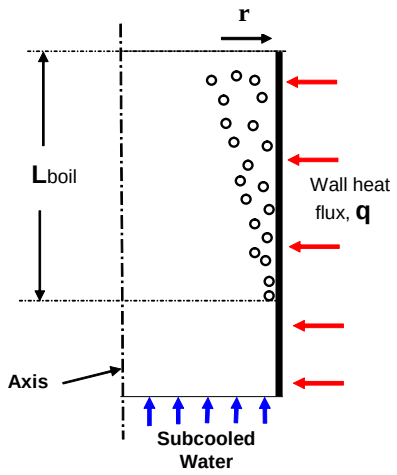

Fig.12. Schematic of the experimental section for study of drag in surface-boiling water

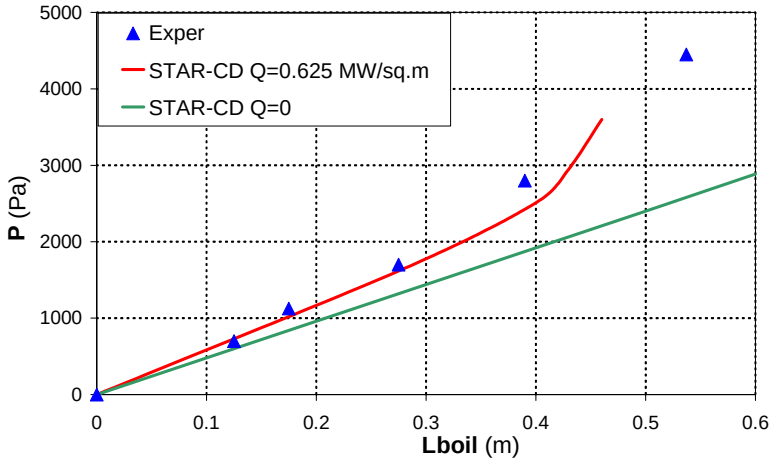

Fig.13. Calculated pressure difference compared to the measurement

2.3 Validation Series C

Bartolemei and Gorburov experiments

Upward flow with condensation of steam in vertical 2 m-long pipe of diameter 32 mm with adiabatic (no-heated walls) was studied in the Bartolemei and Gorburov experiments [19]. Schematic of the experimental section is presented in Fig. 14. A steam-water mixture was created in a mixing chamber attached to the bottom of the pipe. Due to the sub-cooling of the water, steam is condensed as the mixture moves up the pipe. In the experiments the averaged per section void fraction along the pipe was measured, and these data are used for comparison with calculated results.

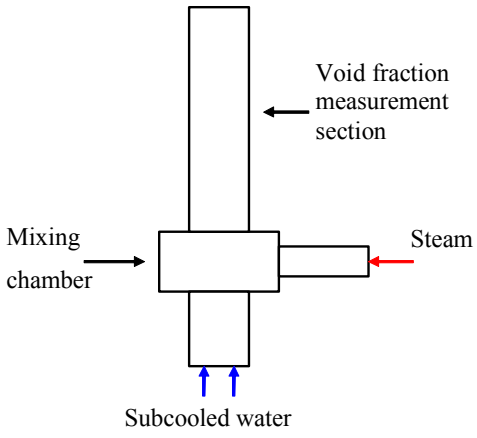

Fig. 14. Schematic of experimental section for study of condensation

Calculations were performed for experiments #5-a and 7-b, parameters of experimental set-up (pressure P, mass flux of water G_l, water sub-cooling and void fraction at the mixing chamber outlet ΔT_{sub} and α) are presented in Table 3.

Table 3. Parameters of experimental set-up

Experiment #	P, Mpa	G_l, kg/(m^2·s)	ΔT_{sub}, K	α
5-a	2	250	15	0.25
7-b	3	420	35	0.4

Inter-phase heat transfer was calculated with constant Nusselt number Nu=2, bubble diameter was assumed constant D_b=2.3 mm corresponding to Nu=2. Results of calculations in comparison with experimental data are presented in Fig. 16 as STAR-CD. Good agreement between numerical and experimental results has been achieved. Discrepancy is observed only at low void fractions.

A possible way to improve the results at low void fractions is to introduce void-fraction-dependent bubble diameter during condensation below a specified threshold void fraction, see Ref. [1]. That is, changing the bubble size in simulation of condensation instead of changing the number of bubbles (as is done in the standard condensation model). Results of these calculations are also presented in Fig. 15 as STAR-CD variable D.

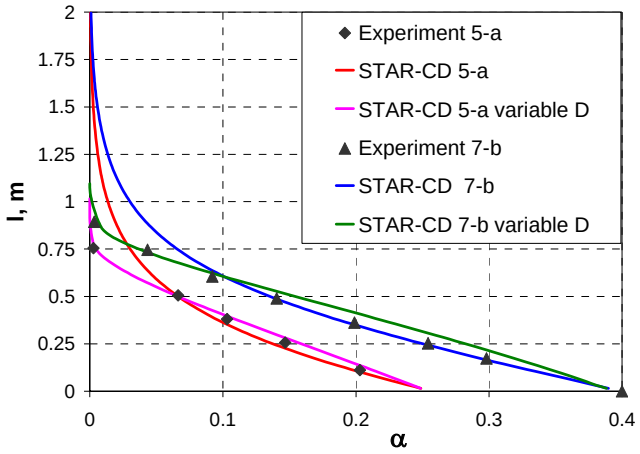

Fig.15. Void fraction as a function of axial distance

2.4 Validation Series D

Koizumi, et al., experiments

Upward steam-water dispersed flow was studied in Koizumi, et al., experiments [20]. The experiments were performed for two set-ups: one rod in a channel (the heated rod in this case was located in a circular pipe, the pipe and the rod being coaxial) and a bundle of 25 rods in a channel of square cross-section. In both cases, steam-water mixture was fed into the measuring channel, and there was no liquid film on the heated rods. Film can develop, however, on lower parts of the rods due to droplet deposition from the flow. Schematic of experimental section for single rod set-up is presented in Fig. 16. In the experiments, axial distributions of rod surface temperature was measured for various wall heat flux: q=346-493 kW/m^2.

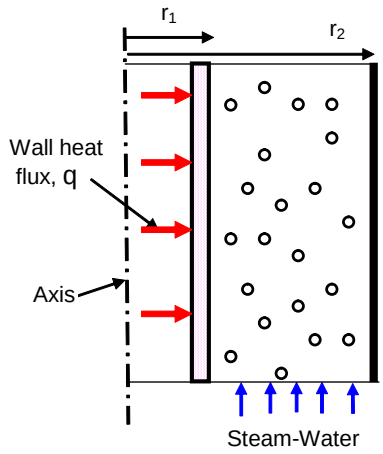

Fig.16. Schematic of experimental section for study of disperse flow

Numerical simulation of single-rod experiments (length of channel 2 m, radius of channel 11 mm, radius of heated rod 6.135 mm) was performed for pressure P=3 MPa, temperature of steam-water mixture and void fraction at inlet T=507 K and α=0.012 and mass flux of mixture G=310 kg/(m^2·s).

Standard STAR-CD models for turbulent dispersion force, virtual mass and lift force were used in the calculations.

Simulated axial distributions of rod surface temperature are presented in Fig. 17 in comparison with experimental data. Note, that liquid film was not modeled numerically. The temperature of the heated rod in simulations starts to rise in the lowest point with heating (the annulus inlet). The coordinate of this point is assumed to be equal to the dry-out point in the experiment. The data shown in Fig. 17 suggest that at q<367 kW/m^2 temperature is over-predicted, while at q>367 kW/m^2 it is under-predicted.

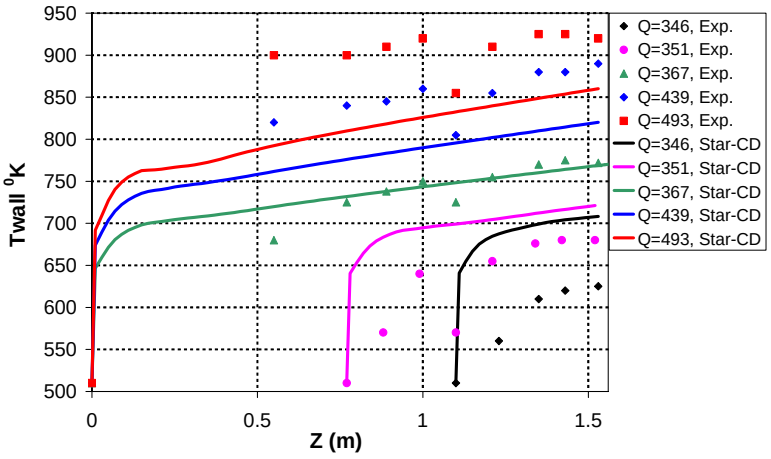

Fig.17. Axial distributions of rod surface temperature

3. Conclusion and Future Model Validation Plans

The CFD-BWR validation plan includes a staged approach with several series of test-cases focused on specific two-phase flow phenomena or integrated experiments. The goal of specific two-phase phenomena analysises is to validateand improve the current models used for the forces, turbulence, bubble and droplet diameter, etc. for all inter-phase surface topologies typical for a BWR fuel assembly. Currently, the validation series **A**, **B** and **C** have been almost completed, and simulations of test-cases series **D** have been started. While the initial validation effort was focused on the bubbly two-phase flow topologies, future work will also validate the models used for other BWR two-phase flow topologies Along with validation of the models of separate two-phase phenomena involved, validation of the code through analyses of integral test-cases (series **I**) that include flow channels with multiple inter-phase surface topologies and rod bundle experiments (series **M**), including bundles with spacers, has been started.

Acknowledgements

This work was performed under partial financial support of ISTC Project #2601p, sponsored by the U.S. Department of Energy IPP Program.

References

[1] Tentner A., Lo S., Ioilev A., Samigulin M., Ustinenko V., Computational fluid dynamics modeling of two-phase flow in a boiling water reactor fuel assembly. Proc. Int. Topical Meeting Mathematics and Computations, Supercomputing, Reactor Physics and Nuclear and Biological Applications M&C-2005, American Nuclear Society, Avignon, France, Sept. 12-15, 2005.
[2] Tentner A., Lo S., Ioilev A., Samigulin M., Ustinenko V., Melnikov V., Kozlov V., Advances in computational fluid dynamics modeling of two phase flow in a boiling water reactor fuel assembly. Proc. Int. Conf. Nuclear Engineering ICONE-14, Miami, Florida, USA, July 17-20, 2006.
[3] STAR-CD Version 3.20 Methodology Manual, Chapter 13, CD-adapco, UK (2004).
[4] Lo S., Modelling multiphase flow with an Eulerian approach. Von Karman Institute Lecture Series - Industrial Two-Phase Flow CFD, May 23-27, von Karman Institute, Belgium (2005).
[5] Ohnuki A., Akimoto H., Model development for bubble turbulent diffusion and bubble diameter in large vertical pipes. J. Nuclear Science Technology, 2001, Vol.38, No.12, p.1074-1080.
[6] Tomiyama A., Tarnai H., Zun I., Hosokama S., Transverse migration of single bubbles in simple shear flow. Chem. Eng. Sci., 2002, Vol.57, p.1849-1858
[7] Troshko A.A., Hassan Y.A., A two-equation turbulent model of turbulent bubbly flows. Int. J. Multiphase Flow, 2001, vol.27, p.1965-2000.
[8] Antal S.P., Lahey R.T., Flaherty J.E., Analysis of phase distribution in fully developed laminar bubbly two phase flow. Int. J. Multiphase Flow, 1991, Vol. 7, p.635-652.
[9] Wang S.K., Lee S.J., Jones O.C., Lahey R.T., 3D turbulence structure and phase distribution measurements in bubbly two-phase flows. Int. J. Multiphase Flow, 1987, Vol.13, No.3, p.327-343.
[10] Liu T.J., The role of bubble size on liquid phase turbulent structure in two-phase bubbly flow. In: Proc. Third International Congress on Multiphase Flow ICMF'98, Lyon, France, June 8-12, 1998. CD ROM Publication.
[11] Serizawa A., Kataoka I., Michiyoshi I., Turbulent structure of air-water bubbly flow. Parts I-III. Int. J. Multiphase Flow, 1975, Vol.2, p.221-259
[12] Bartolemei G.G., Batashova G.N., Brantov V.G., et.al. In: Teplomassoobmen-IV. Vol.5. Minsk. ITMO AN BSSR Press, 1980, p.38.
[13] Avdeev A.A., Pekhterev V.P., Vapour condensation in non-equilibrium bubbly flows. High Temperature, 1986, Vol.24, No.6, p.1125-1131.
[14] Kurul N., Podowski M.Z., Multidimensional effects in sub-cooled boiling. Proc. 9'th Heat Transfer Conference, Jerusalem, 1990.
[15] Lee T.H., Park G.C and Lee D.J., Local flow characteristics of subcooled boiling flow of water in a vertical annulus. Int. J. Multiphase Flow, 2002, Vol.28, p.1351-1368.
[16] Tu J.Y., Yeoh G.H., Development of a numerical model for subcooled boiling flow. Third Int. Conf. CFD in the Minerals and Process Industries CSIRO, Melbourne, Australia, December 10-12, 2003.
[17] Yeoh G.H., Tu J.Y., A unified model considering force balances for departing vapour bubbles and population balance in subcooled boiling flow. Nucl. Engineering Design, 2005, Vol.235, p.1251-1265.
[18] Tarasova N.V., Khlopushin V.I., Boronina J.V., Local drag in surface-boiling water in pipes. High Temperature, 1967, Vol.5, No.1, p.130-136.
[19] Bartolemei G.G.., Gorburov V.I., Experimental study of vapour phase condensation in liquid subcooled below saturation temperature. Heat Production, 1969, No.12, p.58-62.
[20] Koizumi Y., Kumamaru H., Yonomoto T., Tasaka K., Post-dryout heat transfer of high-pressure steam-water two-phase flow in single rod channel and multi rod bundle. Nuclear Engineering and Design, 1987, Vol.99, p.157-165.